SPECIAL SECTION ON TRENDS, PERSPECTIVES AND PROSPECTS OF MACHINE LEARNING
APPLIED TO BIOMEDICAL SYSTEMS IN INTERNET OF MEDICAL THINGS

IEEE *Access*

Multidisciplinary : Rapid Review : Open Access Journal

Image-Alignment Based Matching for Irregular Contour Defects Detection

HAIYONG CHEN[1,2,3], **YUEJIAO CUI**[1], **RUINA QIU**[1], **PENG CHEN**[1,2],
WEIPENG LIU[1,2,4], **KUN LIU**[1,2], **(Member, IEEE)**

[1]School of Artificial Intelligence, Hebei University of Technology, Tianjin 300130, China
[2]Engineering Research Center of Intelligent Rehabilitation and Detecting Technology, Ministry of Education, Tianjin 300130, China
[3]Hebei Control Engineering Technology Research Center, Hebei University of Technology, Tianjin 300130, China
[4]State Key Laboratory for Reliability and Intelligence of Electrical Equipment, Tianjin 300130, China

Corresponding authors: Peng Chen (holmes83@163.com) and Weipeng Liu (liuweipeng@hebut.edu.cn)

ABSTRACT Automatic defect inspection is attractive for high-quality workpiece manufacturing with irregular contours in order to achieve high accuracy and no contour defect. Thus, a novel image alignment-based feature matching algorithm framework is proposed in this paper. It can be used to solve the specified pixel-level defect detection and location problems for workpieces with irregular contours. A new forensic hash is first generated by extracting the scale, position, and main orientation information of feature points. Since the forensic hash is invariant to rotation, translation, and scaling, it is used for feature matching. A feature matching method based on a robust cascade estimator is proposed second to establish an accurate correspondence between the test image and reference image according to the obtained image hash and a parameter space voting mechanism. Third, the matched feature points are used to estimate the similar transformation parameters to achieve an accurate image alignment. Finally, image difference and morphological technique are used to locate the contour defect. Experimental results demonstrate that the proposed algorithm can effectively detect and locate small contour defects in irregular stamping workpieces.

INDEX TERMS Visual inspection, irregular contour, feature matching, image alignment.

I. INTRODUCTION

With the rapid development of manufacturing technology, mechanical workpieces with irregular contours have been widely used in many industrial areas, such as aerospace, automotive vehicles, medical instruments, shipbuilding industries, etc. Nowadays, most workpieces with irregular contours can be automatically manufactured by employing a punching machine; however, the quality inspection is still carried out manually or through experts' subjective evaluation. The drawbacks of manual inspection are slow, costly and inaccurate during mass manufacturing process [1], [2]. The common defects including contour loss have limited their further applications in many manufacturing industries. Furthermore, four difficult problems are unavoidable during manually inspection: 1) the evaluation criteria may be different because of different experts; 2) valuable quality information may be lost which can be used to perform a ''big-data'' analysis so that the statistical features of quality information in predefined production batch can be illustrated; 3) small contour defects may be ignored; 4) defects cannot be accurately located in order to help the maintaining of production equipment in time. Thus, how to simultaneously achieve high efficiency and high production rate is a great challenging issue for producing high-quality workpieces with irregular contours.

Generally, the automatic contour quality inspection through visual sensors can be divided into three categories: 1) contour feature analysis method; 2) shape matching method; 3) image registration method. The first one describes the irregular contour by geometrical features such as length, diameter or distance. In this way, the contour can be projected into one dimensional feature space; therefore the gradient analysis can be used to detect contour defects. The second one compares the shape of the defective workpiece with a standard template and calculates the similarity of the two contours [8]. The third one compares the defective workpiece image with the reference image so that the difference

image will display certain contour defects [9]. Unfortunately, the shortcomings of regular contour defect detection methods prevent them from fulfilling the tasks under the requirement of detecting irregular free-form contour defects [3]–[5].

A few of pioneering studies have been carried out to solve this problem. Fernández, et al. proposed a machine-vision-based method to detect contour defects of inserts. The method can determine if there are edge brokens without requiring reference images of intact inserts [6]. Maddala *et al.* [7] proposed a vision-based measurement approach to detect small defects of the subsequent wear of pills by measuring the radius of the inner and outer rings of pills' contour. In [6] and [7], the defects of regular contour are recognized by using priori knowledge of the regular shape. It means the defects can be detected by analyzing the geometrical features such as length and diameter. However, these methods still cannot be applied directly on the irregular contours. Therefore, some researchers have tried to apply template matching methods based on shape similarity [10]. Normally, two images are required for template matching, one is the reference image, and the other one is the test image. Irregular contour defects can be detected by comparing the shape similarity of contours between two images [11]. Hausdorff distance is a popular similarity metric used in shape matching which can be calculated without explicit point-sets correspondences, but it is sensitive to noises and variations [12]. Some structure features such as curvatures and lengths are often employed to represent the shape, based on these structural features, the overall matching similarity is calculated to evaluate the contour integrity. However, the global-structure-based matching is less sensitive to local deformations or defects. Meanwhile, the precise shape defect detection is difficult because the shape does not possess a unique and stable geometric representation [13]. Monga, et al. proposed an image changing detection framework that employs salient feature points and Hausdorff distance to compare two images. It's robust to most benchmark data, which motivates this study [14]. In order to refine the feature description to improve the accuracy, the boundary-descriptor approach is introduced. The boundary descriptor is robust to rotation, translation, scaling and some other changes [15]. To reduce the matching complexity, Yang, et al. introduced a novel shape descriptor with robust interest point detection. However, some information of small contour defects is lost [16]. Therefore, the method can only solve the problem with obvious defects, it is difficult to distinguish and locate small differences in an irregular contour.

Some researchers have proposed to use image registration techniques to deal with small defects detection problems [17], [18]. Two main challenges for image registration techniques are: 1) the reference image and each test image are usually subject to similar transformation, which makes the two images cannot be well aligned. 2) The intensity of reference image and test image are not exactly the same because the pose of each workpiece relative to the camera and light source is not exactly the same. Therefore, in the original research of Lowe, a reliable feature-based matching

method is proposed to provide control points between image pairs [19]. Goncalves *et al.* [20] improved Lowe's method by adding image segmentation technology to reduce the displacing of control points from their true positions, so that more correct matching points will lead to more accurate image registration results. Because the outliers are unavoidable during the image matching process, a classical method, Random Sample and Consensus (RANSAC) is usually applied to guarantee a correct matching result. Melegy proposed a model-wise and point-wise RANSAC method for robust regression and outline detection [21]. But this method is computationally complex, and the accuracy depends on a large number of parameters. To address this issue, Ma, et al. proposed a non-parametric model-based method based on Progressive Vector Field Consensus (PVFC) [22]. However, the method requires a large putative correspondence set which may lead to inaccurate matches. Xiang *et al.* [23] designed a vector-angle based (VA) algorithm for unconstrained many-objective optimization. The method can improve the matching speed but require more sufficient relevant data. Pun *et al.* [24] proposed a color image alignment-based multi-region matching scheme to precisely locate the differences between images tampering localization. The method firstly segment an image into sufficient regions, and then generate an image hash by encoding color and position information from each region, in order to meet the compactness of relevant data.

To meet the requirement of defect detection of free-form contours, a novel defect detection framework for planar products with irregular contours is proposed in this paper. An image alignment-based feature matching algorithm framework is proposed to generate an accurate, pixel-level defects localization result. The scale, position and main orientation of each point are used as a compact feature representation [26]. The proposed algorithm framework initially establishes the correspondence between the test and reference image. Then a robust cascade estimator based on the main orientation of the image hash and parameter space voting mechanism is presented to estimate the parameters of similar transformation in order to align images. Finally, image difference and morphological technique are utilized to remove the pseudo-defects and only keep the real defects. The contribution of proposed framework is as follows:

1) An image alignment-based feature matching method is proposed as a robust registration strategy between the reference and test image. A novel cascade estimator is designed to obtain more accurate feature matching result in order to estimate the similar transformation parameters for image alignment.

2) A robust image defect detection and location approach is proposed. The residual pseudo-defect after image difference between the reference and test image can be removed by using morphological technique, and the real irregular contour defects can be accurately detected and located.

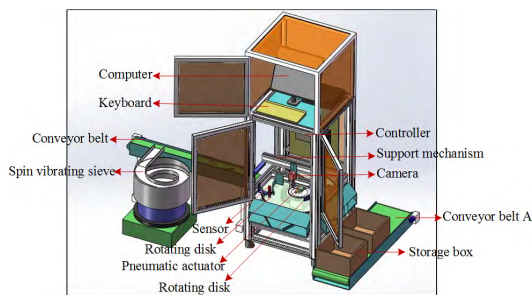3) A complete visual inspection system and algorithm framework is proposed for the contour defect detection

FIGURE 1. Contour defects visual detection system for irregular metal stamping workpiece.
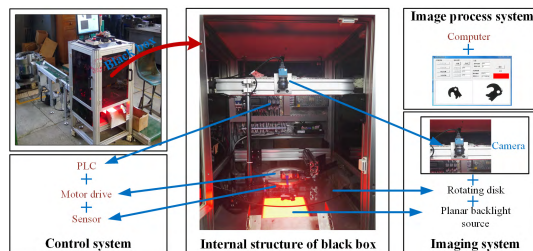

FIGURE 2. Visual inspection system for detection of irregular contour defects.

of irregular stampings. Furthermore, the proposed algorithm framework shows good adaptability to various irregular metal products.

The rest of the paper is organized as follows. Section II focuses on the visual inspection system for irregular contour defects detection. Section III explains the defect detection algorithm framework, which includes feature extraction and rough matching, a robust cascade estimator, image alignment and contour defects location. The experiments and analysis of the results are elaborated in Section IV. Section V provides the final conclusion and future works.

II. VISUAL INSPECTION SYSTEM FOR IRREGULAR CONTOUR DEFECTS

To realize the automatic defect detection, a visual inspection system is designed. Compared with manually defect detection, the designed visual inspection system has the following advantages, such as non-contact, high efficiency, low cost and more accurate. It is specially designed for small contour defects detection of irregular stamping workpieces, its structure is shown in Fig. 1.

The visual inspection system consists of four parts: image acquisition subsystem, image processing subsystem, control subsystem and execution subsystem. The image acquisition subsystem includes high-precision industrial camera, planar backlight source and camera carrier mechanism with multiple degrees of freedom. Where the industrial camera is MER-500-14GM with a resolution of 2592 $\times$ 1944 pixels and the lens' focal length is 16mm. The height of the camera carrier can be adjusted to keep the distance from the camera to the workpiece to be about 280mm forming a view field about 124*mm* $\times$ 93*mm* on the detection plane. A bright red planar backlight source is selected to improve the contrast between background and target workpiece in order to ease the detection of contour defects. Meanwhile, the way of back illumination can also avoid reflection from metal parts. The size of planar backlight source is 160*mm*$\times$160*mm*. The image processing subsystem is composed of an image processing computer and image processing software. The control subsystem consists of a PLC controller, sensors, a motor and its driver, electrical accessories, etc. The execution subsystem includes a spin vibrating sieve, two conveyor belts, a rotating

disk and pneumatic actuators. Some specific snapshots of the visual inspection system are shown in Fig. 2.

The workflow of the visual inspection system is shown in Fig. 3. After startup, the frequency of the spin vibrating sieve is adjusted to 12 Hz. The workpiece to be detected are initially transported to the low speed conveyor belt one by one and then to high speed conveyor belt. By this way, workpieces are evenly sent to the rotating disk because of the speed difference of the two adjacent conveyor belts.

When a workpiece is passed through the electromagnetic induction sensor in front of the camera along the direction of rotation, the sensor will send a workpiece arrival signal to the PLC controller. Then the PLC computes a suitable time interval according to the predefined speed of the rotating disk and the distance between the sensor and the camera. The PLC immediately sends an image capturing trigger signal to the camera, so that the image of the workpiece can be captured by the camera. The captured image is transmitted to the image processing computer. The image processing algorithm framework proposed in this paper is utilized to identify defects of the workpiece. When the number of qualified workpieces reaches a predefined number, the controller sends a signal to control conveyor belt A to move a given distance to make all the qualified workpieces collected by the empty storage box under the discharge gate.

III. VISUAL INSPECTION SCHEME FOR IRREGULAR CONTOUR DEFECTS

The proposed visual inspection algorithm framework consists of three parts: 1) feature extraction and rough matching of feature points, 2) transformation parameters estimation, 3) image alignment and contour defects location. Feature extraction is implemented by using the scale-invariant transformation (SIFT) algorithm. Furthermore, a robust image hash expressed as h is built as the feature descriptor, which has shown superior performance for the scaling, rotation and translation invariance of the feature points. After feature extraction, the rough matching of feature points is realized through calculating similarity of feature descriptors. The similar transformation parameters are estimated by using a cascade estimator combined with the orientation of h and parameter space voting mechanism. The proposed cascade estimator can optimize the matching of feature points to obtain a more accurate correspondence between two images.
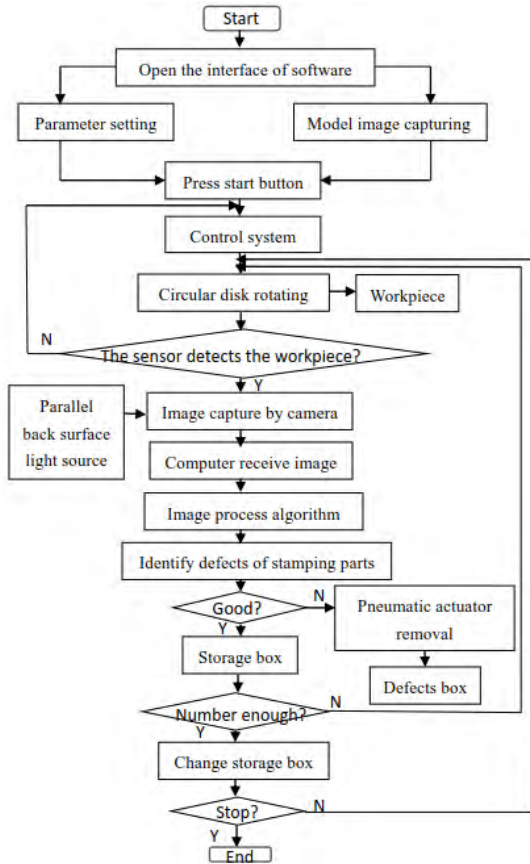
FIGURE 3. Flowchart for detection of irregular contour defects.

FIGURE 4. The overview framework of the proposed algorithm.

Image alignment is achieved by making use of the similar transformation matrix and robust image hash. Finally, the irregular contour defects are located by the image difference and morphological technique after image alignment. The algorithm framework is illustrated in Fig. 4.

The reference image and test image mentioned in this paper are both in BMP format, and the reference image is an image of a qualified irregular stamping workpiece captured in advance, the test image is captured after the camera receives a real-time trigger signal.

A. FEATURE EXTRACTION AND ROUGH MATCHING

Feature extraction mainly includes constructing a scale space, detecting scale space extremum, determining the feature point orientation and generating a description of the feature point. A scale space of an image can be described by the following equation:

$$L(x, y, \sigma) = G(x, y, \sigma) * I(x, y) \quad (1)$$

where the sign '$*$' is the convolution of the Gaussian function $G(x, y, \sigma)$ and image $I(x, y)$, σ is the scale space factor, L is the gauss scale space of the image. The Gaussian function is represented as:

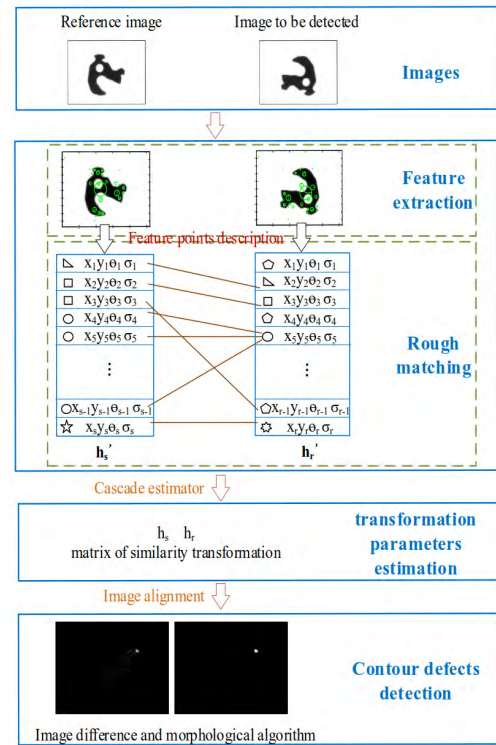$$G(x, y, \sigma) = \frac{1}{2\pi\sigma^2} e^{-(x^2+y^2)/2\sigma^2} \quad (2)$$

However, in real applications, the difference-of-Gaussian (DoG) operator is regarded more efficient, which can be described as:

$$D(x, y, \sigma) = |G(x, y, k\sigma) - G(x, y, \sigma)| * I(x, y) \quad (3)$$

$$D(x, y, \sigma) = L(x, y, k\sigma) - L(x, y, \sigma) \quad (4)$$

Moreover, the classic idea of voting in a parameter space has been used for a long time in Hough transform [27], which motivate our methods. The extrema in DoG scale-space are detected as feature points of an image. The position (x, y) and the scale σ information can be firstly extracted. Secondly, to achieve invariance to rotation, the orientation is specified for each feature point by considering the gradient direction distribution of the neighboring pixels around the feature point (x, y). The gradient direction is defined as:

$$\theta(x, y) = \arctan((L(x, y + 1) - L(x, y - 1))/(L(x + 1, y) - L(x - 1, y))) \quad (5)$$

where, the peak angle in the orientation histogram is treated as the main orientation of the feature point. Thus, a four dimensional vector (x, y, θ, σ) can be obtained, which is a robust image hash to represent the feature point. After acquiring each feature point representation, the next thing is to generate the corresponding descriptor for each feature point. According to SIFT algorithm [19], a 16×16 neighborhood region around the feature point is divided into four 4×4 sub-regions. For every sub-region, an orientation histogram with 8 bins is created. A descriptor vector of 128 dimensions
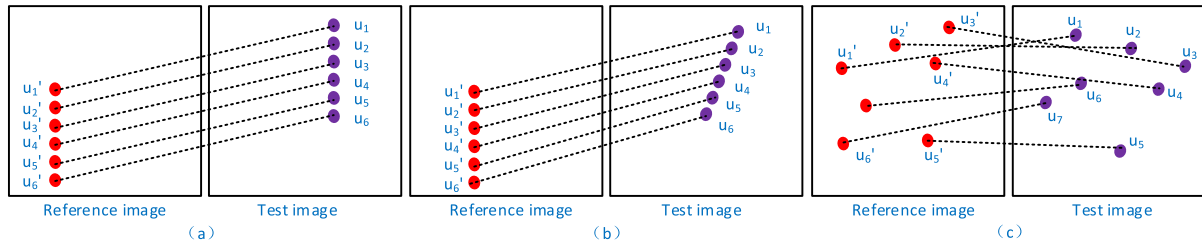
FIGURE 5. Illustration of correspondences between the correctly matched feature point pairs of the reference and test images.

can be acquired by composing the orientation histograms of 16 sub-regions into one column.

In our application, we denote the reference image and test image as I_r and I_t. Therefore, if there are K_r and K_t feature points in I_r and I_t respectively, then image matching will be performed based on the Euclidean distance between K_r and K_t dimensional vectors [17]. Furthermore, the matching result need to be refined in order to remove the replication and false matched feature point pairs depending on certain parameter constraints. However, these parameter constraints are usually different for different reference and test images. Therefore, a robust parameter estimation method is needed.

B. FEATURE MATCHING AND PARAMETER ESTIMATING BASED ON ROBUST CASCADE ESTIMATOR

As aforementioned, the reference image and the test image need to be aligned through 2-D geometric transformation. According to the system setup shown in Fig. 2, geometric transformation can be approximated by similar transformation. After a rough feature matching, a robust consistent linear correspondence between every matched feature point pairs can be applied for estimating similar transformation parameters, as shown in Fig. 5.

In Fig. 5, the red and purple points represent the feature points detected in the reference and test images, respectively. Feature points in the reference image are denoted as u'_i, $i = 1, \ldots, n$, and the corresponding feature points in the test image are denoted as u_i, $i = 1, \ldots, n$. The correspondences between the two feature point sets are represented by the dotted lines in Fig. 5.

Since a correct feature point matching results in a consistent correspondence subject to similar transformation between the two sets of feature points, therefore give a pair of matched feature points, $u = (x_r, y_r)$ and $u' = (x_t, y_t)$, satisfy:

$$\begin{bmatrix} x_r \\ y_r \\ 1 \end{bmatrix} = \begin{bmatrix} g\cos\alpha & -g\sin(\alpha) & T_x \\ g\sin(\alpha) & g\cos\alpha & T_y \\ 0 & 0 & 1 \end{bmatrix} \begin{bmatrix} x_t \\ y_t \\ 1 \end{bmatrix} \quad (6)$$

In Equation(6), α, T_x, T_y, g are similar transformation parameters. To estimate those parameters, a novel cascade estimator based on feature matching and parameter estimating is proposed. Based on the rough feature matching result, the cascade estimator firstly projects the spatial coordinate into a quantified parameter space. Then a voting mechanism is introduced in order to obtain the optimal similar

transformation parameters. Given the consideration that false matched feature points may have a great impact on the voting result; the main orientation of the feature points is introduced into the voting process. Detailed description of the cascade estimator is as the following.

Suppose for image I, after using SIFT feature detection algorithm, a set of feature points can be acquired as $u_I(x, y) = \{u_i\}_{i=1}^{N_I}$, where N_I is the number of feature-points in Image I. Every feature point in the set $u_I(x, y)$ can be represented by a four dimensional vector (x, y, θ, g). Therefore, the set $u_I(x, y)$ can be used to form a global vector $h_I = \{(x_i, y_i, \theta_i, g_i)\}_{i=1}^{N_I}$, which can be considered as an image hash and used in the cascade estimator.

According to Equation (6), the following relationship can be acquired:

$$\frac{x_r - T_x}{y_r - T_y} = \frac{x_t \cos\alpha - y_t \sin\alpha}{x_t \sin\alpha + y_t \cos\alpha} \quad (7)$$

Furthermore, Equation (7) can be rewritten as:

$$T_x = \frac{x_t \cos\alpha - y_t \sin\alpha}{x_t \sin\alpha + y_t \cos\alpha}(T_y - y_r) + x_r \quad (8)$$

$$T_y = \frac{x_t \sin\alpha + y_t \cos\alpha}{x_t \cos\alpha - y_t \sin\alpha}(T_x - x_r) + y_r \quad (9)$$

It means that the image coordinate system can be projected to a parameter space coordinate system of $\alpha \times T_x \times T_y$. For a fixed value of α, Equation (8) and Equation (9) indicate that every pair of matched feature points corresponds to two lines in the parameter space. Therefore, a line cluster can be formed by using all the matched feature point pairs, and the parameter vector $\alpha \times T_x \times T_y$ can be initially obtained by finding the mostly intersected points in the parameter space as shown in Fig. 6.

In Fig. 6, each pair of feature point coordinates (x_t, y_t) and (x_r, y_r) votes for a line in the quantized 2D parameter space. Actually, (8) and (9) represent the same line in different ways. Therefore, each matched feature point pair is used twice in the estimation process. During the voting process, lines that do not intersect at the peak should be discarded. Whilst, lines intersecting at the correct peak generated by false matched pairs should also be disregarded in order to avoid forming the false peak in the parameter space. Based on this consideration, the main orientation of feature points is introduced into the voting mechanism to form a cascade estimator. The difference $\Delta\theta = \theta_{r'} - \theta_{t'}$ between the main orientation
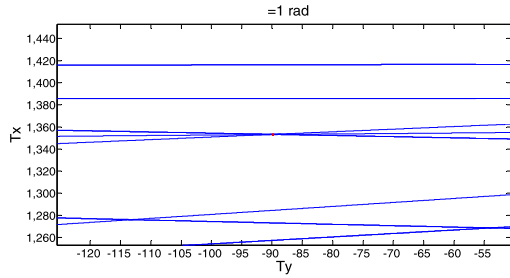
FIGURE 6. A slice of the parameter space when $\alpha = 1$.

of image hashes $h_{t'}$ and $h_{r'}$ is calculated. In the cascade estimator, it is required that $\Delta\theta$ should satisfy $|\Delta\theta - \alpha| < T_\alpha$ where α is the rotation value. By using the cascade estimator, some false matched feature point pairs can be eliminated, so that the voting peak in the parameter space can be located more accurately. To refine the estimation accuracy of the similar transformation parameters, the remaining matching pairs

$$((x_{t(i)}, y_{t(i)}), (x_{r(i)}, y_{r(i)})), \quad N \leq \min(K_t, K_r)i \leq N$$

and the vector (α, T_x, T_y) are used again to estimate the similar transformation parameters, where N is the number of the remaining matching pairs after using the cascade estimator. Specifically, the translation vector between each pair of matched feature points satisfied the following relationship:

$$(T_{x(i)}, T_{y(i)})$$
$$= ((\frac{x_{t(i)} \cos\alpha - y_{t(i)} \sin\alpha}{x_{t(i)} \sin\alpha + y_{t(i)} \cos\alpha}(T_y - y_{r(i)}) + x_{r(i)}), T_y) \quad (10)$$
$$(T_{x(i)}, T_{y(i)})$$
$$= (T_x, (\frac{x_{t(i)} \sin\alpha + y_{t(i)} \cos\alpha}{x_{t(i)} \cos\alpha - y_{t(i)} \sin\alpha}(T_x - x_{r(i)}) + y_{r(i)})) \quad (11)$$

Where, $(T_{x(i)}, T_{y(i)})$ is the translation vector. Meanwhile, every matched pair should also satisfy:

$$x_{r(i)} = x_{t(i)}g_{(i)} \cos\alpha_{(i)} - y_{t(i)}g_{(i)} \sin\alpha_{(i)} + T_{x(i)} \quad (12)$$
$$y_{r(i)} = x_{t(i)}g_{(i)} \sin\alpha_{(i)} + y_{t(i)}g_{(i)} \cos\alpha_{(i)} + T_{y(i)} \quad (13)$$

Solving Equation (12) and Equation (13) by employing $a_i = g_{(i)} \cos\alpha_{(i)}$, $b_i = g_{(i)} \sin\alpha_{(i)}$:

$$a_i = \frac{y_{r(i)}y_{t(i)} + x_{r(i)}x_{t(i)} - x_{t(i)}T_{x(i)} - y_{t(i)}T_{y(i)}}{x_{t(i)}^2 + y_{t(i)}^2} \quad (14)$$

$$b_i = \frac{x_{t(i)}y_{r(i)} - x_{r(i)}y_{t(i)} + y_{t(i)}T_{x(i)} - x_{t(i)}T_{y(i)}}{x_{t(i)}^2 + y_{t(i)}^2} \quad (15)$$

Where $\tan\alpha_{(i)}$ equals to b_i/a_i. The $\alpha_{(i)}$ for each pair of matched feature points are estimated as the following:

$$\alpha_{(i)} = \arctan(\frac{x_{t(i)}y_{r(i)} - x_{r(i)}y_{t(i)} + y_{t(i)}T_{x(i)} - x_{t(i)}T_{y(i)}}{y_{r(i)}y_{t(i)} + x_{r(i)}x_{t(i)} - x_{t(i)}T_{x(i)} - y_{t(i)}T_{y(i)}}) \quad (16)$$

Once $\alpha_{(i)}$ is obtained, (17) can be used to estimate $g_{(i)}$:

$$g_{(i)} = \frac{1}{2} \frac{x_{r(i)} - T_{x(i)}}{x_{t(i)} \cos\alpha_{(i)} - y_{t(i)} \sin\alpha_{(i)}}$$
$$+ \frac{1}{2} \frac{y_{r(i)} - T_{y(i)}}{x_{t(i)} \sin\alpha_{(i)} + y_{t(i)} \cos\alpha_{(i)}} \quad (17)$$

The N parameter vectors $(\alpha_{(i)}, T_{x(i)}, T_{y(i)}, g_{(i)})$ can be obtained through the above process by using N matched feature point pairs and the initial voting result of (α, T_x, T_y) in the parameter space. The more robust similar transformation parameters can be obtained by taking the average of the N parameter vectors:

$$(\alpha, T_x, T_y, g) = (\overline{\alpha_{(i)}}, \overline{T_{x(i)}}, \overline{T_{y(i)}}, \overline{g_{(i)}}) \quad (18)$$

As stated in the reference [24], the direct estimation of g is unreliable due to the replication of the matched pairs. But the replications of matched feature point pairs are helpful for estimating α. Therefore, in the proposed cascade estimator, the replication of matched feature point pairs are maintained, and the information of image hash including spatial position of feature points and their main orientations are considered to make the estimation of α more reliable. Finally, the g can be estimated after using the cascade estimator.

C. IMAGE ALIGNMENT AND CONTOUR DEFECTS LOCATION

Obtained the similar transformation parameters (α, T_x, T_y, g), the transformation matrix can be reconstructed according to Equation (6) as the following:

$$\mathbf{T} = \begin{bmatrix} g\cos\alpha & -g\sin\alpha & T_x \\ g\sin\alpha & g\cos\alpha & T_y \\ 0 & 0 & 1 \end{bmatrix} \quad (19)$$

Therefore, to align a feature point $u' = (x_t, y_t)$ in the reference image to a feature point $u = (x_r, y_r)$ in the test image, we can apply the following equation:

Denote the image obtained from the reference image after alignment according to Equation (20) as $I_{rm}(x, y)$.

$$\begin{bmatrix} x_r \\ y_r \\ 1 \end{bmatrix} = \mathbf{T} \begin{bmatrix} x_t \\ y_t \\ 1 \end{bmatrix} \quad (20)$$

To extract the contour defects, the difference between the real test image $I_t(x, y)$ and the image $I_{tm}(x, y)$ is calculated as:

$$d_{t,tm}(x, y) = \begin{cases} 1 & |I_t(x, y) - I_{tm}(x, y)| > TH \\ 0 & others \end{cases} \quad (21)$$

where TH is a predefined threshold, $d_{t,tm}(x, y)$ can be treated as a binary image which contains contour defects, edge differences and pseudo-defects because of the tiny thickness varying or shape varying between different workpieces. Therefore, morphological opening operation is introduced to remove the pseudo-defects, in order to ensure accurate extraction and location of the real irregular contour defects.

TABLE 1. Feature matchin g statistics.

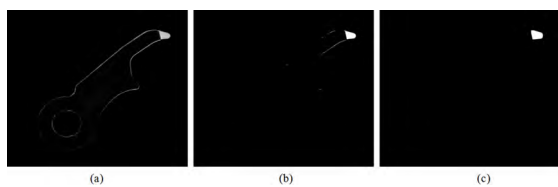| Method	Number of SIFT feature points (template image test image)		Number of matching pairs	Number of mismatching pairs
Algorithm in [21]	68	27	13	8
Algorithm in [23]	68	27	15	4
Algorithm in [25]	68	27	9	5
Proposed method	68	27	6	0

FIGURE 7. Analysis results of the difference operation and morphological operation (a) difference image after image alignment (b) the binary image of contour defects after thresholding (c) contour defects after using morphological operation.
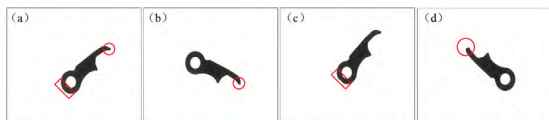

FIGURE 8. Irregular stamping workpieces.

FIGURE 9. Feature detection results.

The experimental results of the difference operation and morphological operation are shown in Fig. 7.

In Fig. 7 (a) and (b), both pseudo-defects and real defects are presented. After using the morphological operation, the pseudo-defects are removed and only the real defects are retained in Fig. 7 (c).

IV. EXPERIMENTAL RESULTS AND ANALYSIS

To verify the effectiveness of the proposed algorithm framework, the images of stamping workpieces with different contour defects are collected, as shown in Fig.8. The thickness of the stamping workpieces is around 3.2mm, and the image resolution is 2592 × 1944. Fig. 8 (a) is an image of the standard stamping workpieces, (b)-(d) are images of stamping workpieces with different contour defects,

where the defects are highlighted with red marks in each image. For every irregular stamping workpiece, the detected feature points including their position, scale and the main orientation are shown in Fig. 9.

As shown in Fig. 9, the size of the red circle in the image is proportional to the scale of a feature point, the arrow line indicates the orientation of a feature point.
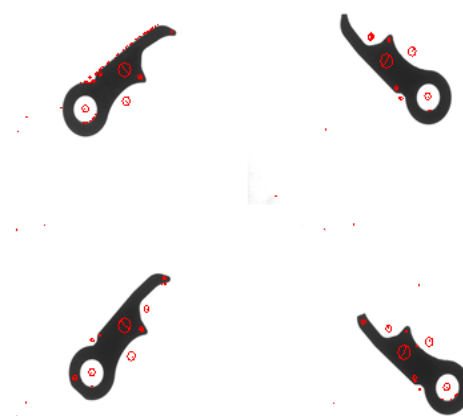
Since one of our contribution is improving the SIFT algorithm based on the robust cascade estimator to achieve robust image alignment, the performance of the improved algorithm is compared to the typical algorithms described in [21], [23], and [25] in the following experiments. As shown in Fig. 10, feature matching results in column (d) have the most correct connections between the two corresponding feature point sets of the reference image and test image.

It indicates that the proposed algorithm in this paper can achieve more accurate feature matching result than the algorithms proposed in [21], [23], and [25], so that the proposed algorithm can be used to acquire more accurate estimation of the similar transformation parameters. Furthermore, another 25 test images are used to evaluate the performance of the above algorithms, the average feature matching and mismatching results are shown in TABLE 1.

As shown in TABLE 1, although the algorithms in [21], [23], and [25] can find more matching point pairs, but the number of false matches is also high. On the contrast, the proposed algorithm can find less matching point pairs, but every point pair can be matched correctly. Therefore, the proposed algorithm is more suitable for establishing an accurate correspondence between the test image and reference image.
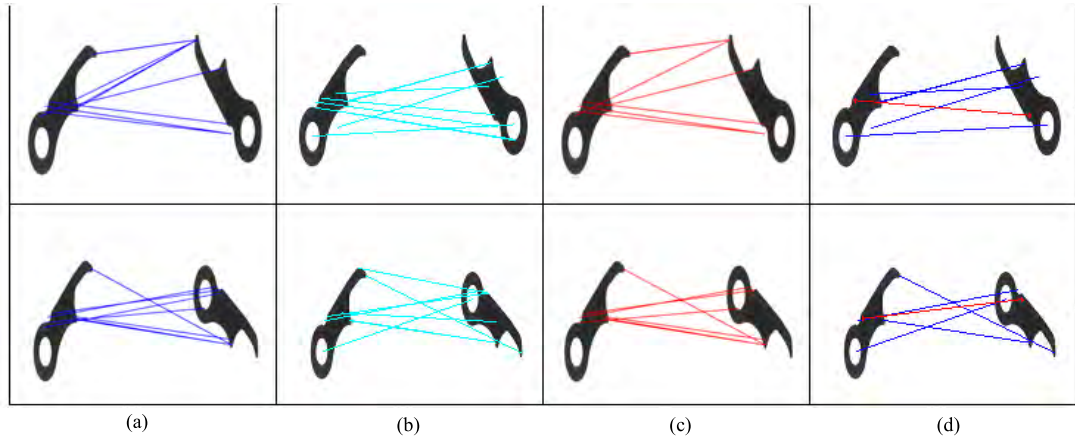
FIGURE 10. Feature matching. (a) Algorithm referenced in [21] (b) VA algorithm in [23] (c) FLANN algorithm in [25] (d) The proposed algorithm.
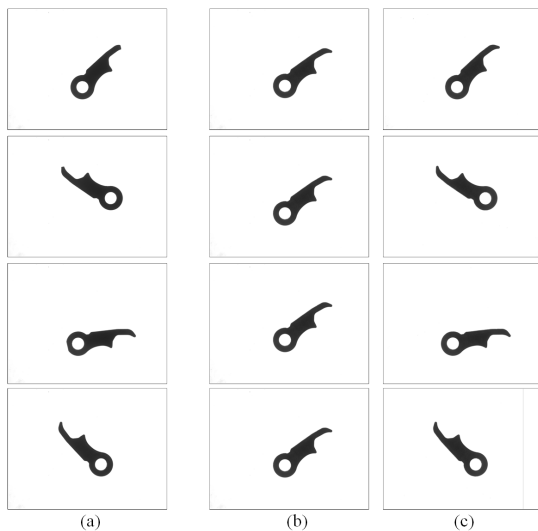

FIGURE 11. Result of image alignment (a) test image (b) reference image (c) results of applying similar transformation on the reference image.

After acquiring the matched feature point pairs, the similar transformation parameters $(\alpha, T_x, T_y, \sigma)$ can be estimated according to Equation(17)-(19). To achieve an accurate alignment of the test image and the reference image, the estimated similar transformation can be applied to the reference image, in order to the make the workpiece in the reference image have the same orientation as the one in the test image as shown in Fig.11.

According to Equation (21), image difference is firstly performed between the test image and the transformed reference image. Then, thresholding operation is performed on the difference image, so that a binary image with contour defects and pseudo-defects can be obtained. Morphological operation is finally employed on the binary image to remove pseudo-defects. A large number of experiments have been carried out, and some experimental results are shown in Fig. 12 and Fig. 13.

TABLE 2. Defect detection performance on test samples.

Method	True Positive Rate	True Negative Rate	False Negative Rate	time
Algorithm in [28]	90.6%	7.1%	2.3%	1.13s
Proposed method	97%	2.4%	0.6%	0.83s

As shown in Fig. 12 and Fig. 13, the proposed algorithm framework can effectively realize the robust image alignment and accurately identify the contour defect of irregular stamping workpiece. In order to further verify the effectiveness of the proposed algorithm framework, more experiments are carried out on a PC with Intel Core 3.6 GHz CPU and 8GB memory. 500 images with different contour defects are collected. There are 100 defective images in these 500 test images. The defect detection results are categorized as: 1) if a stamping workpiece is correctly detected, then it is called true positive; 2) if a qualified stamping workpiece is detected as defective workpiece, then it is called true negative; 3) if a defective stamping workpiece is detected as a qualified workpiece, then it is called false positive. The true positive rate TP_r, true negative rate TN_r, false positive rate FP_r are specifically defined as:

$$TP_r = \frac{x}{N}; \quad TN_r = \frac{y}{N}; \quad FN_r = \frac{z}{N} \qquad (22)$$

Where N is the total number of samples, x, y, z are the number of true positive, true negative and false negative, respectively. In the experiments, the algorithms in [21], [23], and [25] are usually difficult to obtain a correct alignment result, leading to a low detection rate. However, the proposed algorithm can achieve a detection result up to 97%, as shown in TABLE 2. Small defects or noise interference may cause false detection in the test images. In order to illustrate the
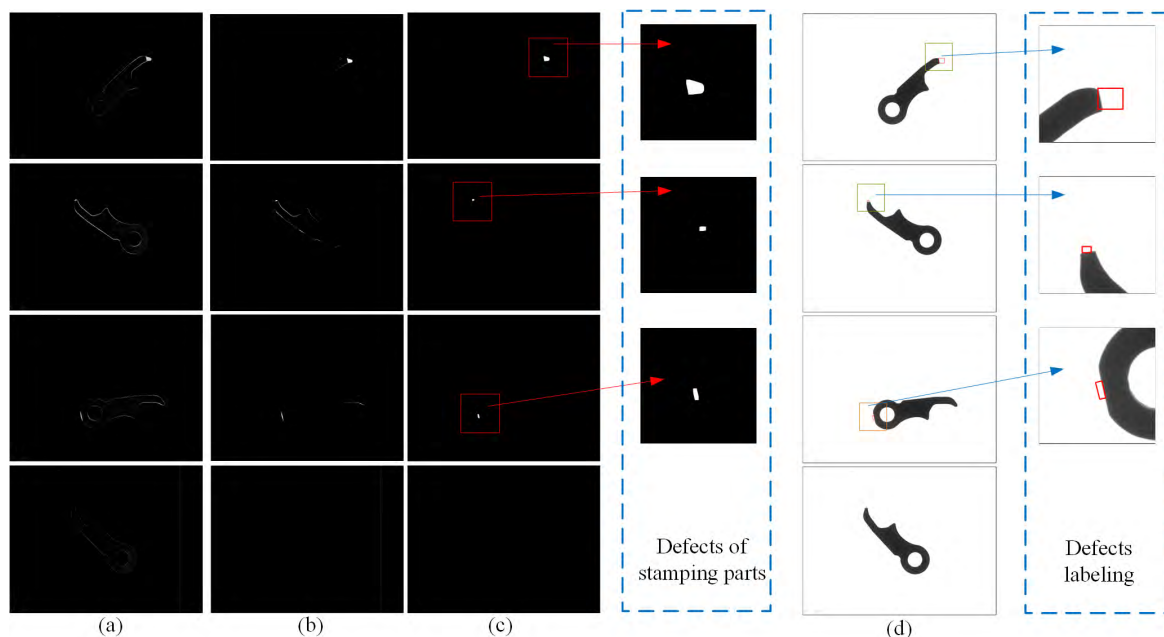
FIGURE 12. The smaller irregular contour defects detection (a) the difference image (b) the binary image after thresholding (c) the defect extraction result after the morphological operation (d) defects labeling.

FIGURE 13. Small irregular contour defects detection (a) the difference image (b) the binary image after thresholding (c) the defect extraction result after the morphological operation (d) defects labelin.
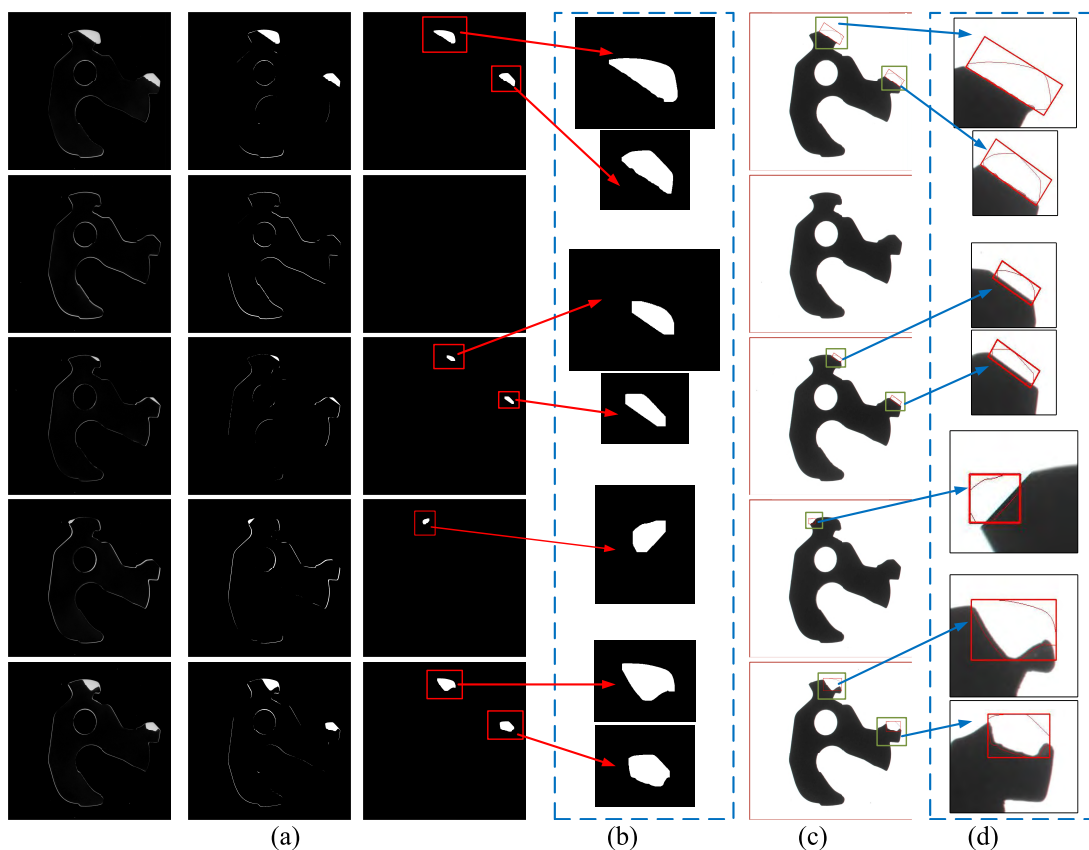
superior performance of the proposed algorithm, the defect detection results by using a contour matching method based on Hu moments [28] are also listed in TABLE 2.

V. CONCLUSION

To assess the quality of products with irregular contours more accurately and objectively, a visual inspection system

based on an alignment-based feature matching algorithm framework was proposed. A robust hash encoding of the position, scale and main orientation information of each feature point was designed to represent the geometric distribution of feature point information. A robust image alignment method based on feature matching was presented. To solve the problem of false matching of traditional feature matching method, a novel cascade estimator based on the main orientation of image hash and parameter space voting mechanism was proposed. Experimental results show that the proposed algorithm framework can achieve an accurate feature matching result, therefore the similar transformation parameters can be estimated more accurately, which certainly helps to realize a robust image alignment. Meanwhile, the proposed algorithm framework shows strong adaptability, it is suitable for a variety of irregular parts. Furthermore, by applying the proposed visual inspection system, the quantization data of contour defects and the image with the defect labeling can be recorded to help discovering the malfunction of the production equipment, which is helpful for improving the quality of the product, as well as the maintenance of the equipment.

REFERENCES

[1] H. Feng, Z. Jiang, F. Xie, P. Yang, J. Shi, and L. Chen, "Automatic fastener classification and defect detection in vision-based railway inspection systems," *IEEE Trans. Instrum. Meas.*, vol. 63, no. 4, pp. 877–888, Apr. 2014.

[2] M. Layouni, M. S. Hamdi, and S. Tahar, "Detection and sizing of metal-loss defects in oil and gas pipelines using pattern-adapted wavelets and machine learning," *Appl. Soft Comput.*, vol. 52, pp. 247–261, Mar. 2017.

[3] T. Li, L. Gao, Q. Pan, and P. Li, "Free-form surface parts quality inspection optimization with a novel sampling method," *Appl. Soft Comput.*, vol. 62, pp. 550–570, Jan. 2018.

[4] Z.-Y. Jia, J.-W. Ma, D.-N. Song, F.-J. Wang, and W. Liu, "A review of contouring-error reduction method in multi-axis CNC machining," *Int. J. Mach. Tools Manuf.*, vol. 125, pp. 34–54, Feb. 2017.

[5] J. Molina, J. E. Solanes, L. Arnal, and J. Tornero, "On the detection of defects on specular car body surfaces," *Robot. Comput.-Integr. Manuf.*, vol. 48, pp. 263–278, Dec. 2017.

[6] L. Fernández-Robles, G. Azzopardi, E. Alegre, and N. Petkov, "Machine-vision-based identification of broken inserts in edge profile milling heads," *Robot. Comput. Integr. Manuf.*, vol. 44, pp. 276–283, Apr. 2017.

[7] T. M. Kanakam *et al.*, "Adaptable ring for vision-based measurements and shape analysis," *IEEE Trans. Instrum. Meas.*, vol. 66, no. 4, pp. 746–756, Apr. 2017.

[8] H. M. Haniff *et al.*, "Shape-based matching: Defect inspection of glue process in vision system," *IEEE Ind. Electron. Appl.*, vol. 470, no. 8, pp. 53–57, 2010.

[9] J.-X. Huang, D. Li, F. Ye, and Z.-J. Dong, "Flexible printed circuit defective detection based on image registration," in *Proc. IEEE Int. Congr. Image Signal Process.*, vol. 6, Oct. 2010, pp. 2570–2574.

[10] O. van Kaick, H. Zhang, G. Hamarneh, and D. Cohen-Or, "A survey on shape correspondence," *Comput. Graph. Forum*, vol. 30, no. 6, pp. 1681–1707, 2011.

[11] J. Yang, H. Wang, J. Yuan, Y. Li, and J. Liue, "Invariant multi-scale descriptor for shape representation, matching and retrieval," *Comput. Vis. Image Understand.*, vol. 145, pp. 43–58, Apr. 2016.

[12] Q. Wei, X. Liang, and F. Jiancheng, "A new star identification algorithm based on improved Hausdorff distance for star sensors," *IEEE Trans. Aerosp. Electron. Syst.*, vol. 49, no. 3, pp. 2101–2109, Jul. 2013.

[13] T. Adamek and N. E. O'Connor, "A multiscale representation method for nonrigid shapes with a single closed contour," *IEEE Trans. Circuits Syst. Video Technol.*, vol. 14, no. 5, pp. 742–753, May 2004.

[14] V. Monga, D. Vats, and B. L. Evans, "Image authentication under geometric attacks via structure matching," in *Proc. IEEE Int. Conf. Multimedia Expo*, Jul. 2005, pp. 229–232.

[15] L. Zhao, Q. Peng, and B. Huang, "Shape matching algorithm based on shape contexts," *IET Comput. Vis.*, vol. 9, no. 5, pp. 681–690, Oct. 2015.

[16] C. Yang, C. Feinen, O. Tiebe, K. Shirahama, and M. Grzegorzek, "Shape-based object matching using interesting points and high-order graphs," *Pattern Recognit. Lett.*, vol. 83, pp. 251–260, Nov. 2016.

[17] S. Battiato, G. M. Battiato, E. Farinella, E. Messina, and G. Puglisi, "Robust image registration and tampering localization exploiting bag of features based forensic signature," in *Proc. 19th ACM Int. Conf. Multimedia*, 2011, pp. 1245–1248.

[18] Y. Wu, W. Ma, M. Gong, L. Su, and L. Jiao, "A novel point-matching algorithm based on fast sample consensus for image registration," *IEEE Geosci. Remote Sens. Lett.*, vol. 12, no. 1, pp. 43–47, Jan. 2015.

[19] D. G. Lowe, "Distinctive image features from scale-invariant keypoints," *Int. J. Comput. Vis.*, vol. 60, no. 2, pp. 91–110, 2004.

[20] H. Goncalves, L. Corte-Real, and J. A. Goncalves, "Automatic image registration through image segmentation and SIFT," *IEEE Trans. Geosci. Remote Sens.*, vol. 49, no. 7, pp. 2589–2600, Jul. 2011.

[21] M. T. El-Melegy, "Model-wise and point-wise random sample consensus for robust regression and outlier detection," *Neural Netw.*, vol. 59, no. 11, pp. 23–35, Nov. 2014.

[22] J. Ma, Y. Ma, J. Zhao, and J. Tian, "Image feature matching via progressive vector field consensus," *IEEE Signal Process. Lett.*, vol. 22, no. 6, pp. 767–771, Jun. 2015.

[23] Y. Xiang, Y. Zhou, M. Li, and Z. Chen, "A vector angle-based evolutionary algorithm for unconstrained many-objective optimization," *IEEE Trans. Evol. Comput.*, vol. 21, no. 1, pp. 131–152, Feb. 2017.

[24] C.-M. Pun, C. P. Yan, and X.-C. Yuan, "Image alignment-based multi-region matching for object-level tampering detection," *IEEE Trans. Inf. Forensics Security*, vol. 12, no. 2, pp. 377–391, Feb. 2016.

[25] J. F. Li *et al.*, "Improved SURF detection combined with dual FLANN matching and clustering analysis," *Appl. Mech. Mater.*, vol. 556, pp. 2792–2796, May 2014.

[26] S. Battiato, G. M. Farinella, E. Messina, and G. Puglisi, "Understanding geometric manipulations of images through bovw-based hashing," in *Proc. IEEE Int. Conf. Multimedia Expo*, Jul. 2011, pp. 1–6.

[27] D. H. Ballard, "Generalizing the Hough transform to detect arbitrary shapes," *Pattern Recognit.*, vol. 13, no. 2, pp. 111–122, 1981.

[28] A. Cunha, T. Adão, and P. Trigueiros, "HelpmePills: A mobile pill recognition tool for elderly persons," *Procedia Technol.*, vol. 16, pp. 1523–1532, 2014.

HAIYONG CHEN received the M.S. degree from the Harbin University of Science and Technology, Harbin, China, in 2005, and the Ph.D. degree from the Institute of Automation, Chinese Academy of Sciences, Beijing, China, in 2008.

He is currently a Professor with the School of Artificial Intelligence, Hebei University of Technology, Tianjin, China. His research interests include image processing, robot vision, and pattern recognition.

YUEJIAO CUI received the B.S. degree from the Agricultural University of Hebei, Hebei, China, in 2016.

She is currently pursuing the M.S. degree with the School of Artificial Intelligence, Hebei University of Technology, Tianjin, China. Her current research interests include computer vision pattern recognition and machine learning.

RUINA QIU received the B.S. degree from the Hebei University of Science and Technology, Hebei, China, in 2015.

She is currently pursuing the M.S. degree in automation with the School of Artificial Intelligence, Hebei University of Technology, Tianjin, China. Her current research interests include computer vision, pattern recognition, and machine learning.

WEIPENG LIU received the Ph.D. degree from the Hebei University of Technology, Tianjin, China, in 2016.

He is currently an Associate Professor with the School of Artificial Intelligence, Hebei University of Technology, Tianjin, China. His research interests include image processing, artificial intelligence, and robotics and pattern recognition.

PENG CHEN received the M.S. and Ph.D. degrees from the University of Science and Technology Beijing, Beijing, China, in 2009 and 2015, respectively.

He is currently a Lecturer with the School of Artificial Intelligence, Hebei University of Technology, Tianjin, China. His research interests include 3D reconstruction, SLAM, machine vision, and pattern recognition.

KUN LIU received the M.S. degree from the Harbin Institute of Technology, Harbin, China, in 2003, and the Ph.D. degree in automation from Tsinghua University, Beijing, China, in 2009.

She is currently an Associate Professor with the School of Artificial Intelligence, Hebei University of Technology, Tianjin, China. Her research interests include image processing, computer vision, and pattern recognition.

. . .